Proceedings of CECNet 2022
A.J. Tallón-Ballesteros (Ed.)

doi:10.3233/FAIA220577

Image Restoration of an Object Viewed Through a Polycapillary X-Ray Lens with Square Channels Using the Concept of a Space-Variant Point-Spread Function

Mo ZHOU[a,c], Yiming WU[a,c], Kai PAN[a,c], Zelin DU[a,c], Tiancheng YI[e], Tianxi SUN[a,c,d], Zhiguo LIU[a,b,c,d] and Yude LI[a,b,c,d,1]

[a] *College of Nuclear Science and Technology, Beijing Normal University, Beijing 100875, China*
[b] *Beijing Key Laboratory of Applied Optics, Beijing 100875, China*
[c] *Key Laboratory of Beam Technology, Ministry of Education, Beijing 100875, China*
[d] *Beijing Radiation Center, Beijing 100875, China*
[e] *Spallation Neutron Source Science Center, Dongguan, 523803, Guangdong, China*

Abstract. A polycapillary X-ray lens with square channels is a type of new X-ray optical device that is suitable for both X-ray focusing and imaging. Similar to micropore optics (MPO), the square matrix array of this lens contributes to the good correspondence between each individual channel and each pixel of a position-sensitive detector. The tiny difference in the curvature of each channel makes the point-spread function of this lens spatially variant. To realize image restoration of the raw data viewed through this lens, a Slice method called the Lucy-Richardson overlap-save method using total variation (LROS-TV) was used. In this work, a series of simulations were conducted to investigate at what flux and contrast levels the image features of an object can be resolved. A simple coaxial imaging experiment was also conducted to verify the LROS-TV method by changing the current of the X-ray tube from 300 to 600 μA. In this paper, it was found that the slice method is suitable for image restoration of an object viewed through a polycapillary X-ray lens with square channels.

Keywords. X-ray optics, polycapillary X-ray lens with square channels

1. Introduction

The polycapillary X-ray lens was first proposed by M.A. KUMAKHOV in 1986. [1] This device is a monolithic system fabricated from microstructure glass consisting of a large number of capillary channels. It can be used as an effective collection, focusing, and transfer optic based on the principle of total external reflection. [2] Traditional polycapillary X-ray lenses are not standardized optical imaging elements, although there have been reports on their application to imaging [3-4], especially combining the coded aperture concept, which was proposed recently [5-6]. Inspired by micropore optics (MPO), the optical structure of a polycapillary X-ray lens with square channels was

[1]Corresponding Author: Yude LI, E-mail: liyude@bnu.edu.cn.

presented [7] to overcome the disadvantages caused by the triangular-shaped nonfunctional spaces between the circular channels. Then, slices with square channels that aimed to compose a novel lens using a stack-like arrangement were produced. The characteristic cruciform point-spread function (PSF) was demonstrated experimentally.[8]

Similar to an MPO, the square matrix array of capillaries in a square polycapillary X-ray lens contributes to the good correspondence between each individual channel of the optic device and each pixel of the position-sensitive detector. In this case, a square polycapillary X-ray lens has potential in X-ray imaging analysis applications. In 2000, Andrew G. Peele used the maximum likelihood method in the deconvolution of images viewed with a lobster-eye telescope, for an extended object. [9] For an MPO, the PSF remains consistent irrespective of manufacturing defects. However, for a polycapillary X-ray lens with square channels, individual square channels in different layers are bent, and the outline can be viewed as parabolic. This causes the PSF of this lens to be spatially variant. Various solutions for the restoration of images viewed through an optical system with spatially variant PSFs have been proposed, including sectioned methods [10-11], [12] and monolithic methods [13-14]. Combined with these methods, it is meaningful to demonstrate that image features can be recovered from the raw data collected by a polycapillary X-ray lens with square channels.

In this work, during the simulations, we selected a simple text as the test object. We sectioned the geometry of a thick lens slice and calculated the PSFs in different sections using our verified model. [7] Over the right modeled spatially variant PSFs, we completed the restoration of the raw images obtained using the square polycapillary X-ray lens with the Lucy-Richardson overlap-save method using total variation (LROS-TV). Several simulations were performed to research the influences of the ratio of the object luminous flux to the background and the entrance photon level on the recovered image quality. In addition, an image restoration experiment was implemented to verify the correctness of the simulations. The results of the simulations and experiment indicate that this method is suitable for image restoration when this type of X-ray optical device is used as a lens for imaging transmission.

2. Related Methods

2.1. Calculation of the spatially variant PSFs

The point spread function (PSF) is the response of an imaging system to a point source or point object. As Fig. 1(a) shows, the curvature of the outline of an individual bent channel changed slightly as the layer number increased. Computing the real PSFs of this optic would be very time-consuming. In this case, we simplified the problem by sectioning the geometry of the optic into $N \times N$ parts (Fig. 1(b)). For each section, the channels assumed to be associated with the same PSF kernel for tiny variations in their curvature are negligible. A window of size $r \times r$ was extracted around the center of each section to save the PSF. To calculate the spatially variant PSFs of a polycapillary X-ray lens with square channels, a point source was placed at the center of the transverse plane of each section and at a long distance from the entrance of the optic in the longitudinal direction. As shown in Fig. 2, the X-ray photons emitted from the source isotropic. Then, the process of the ray transmission through each section of the lens was calculated using

the mathematical model of our prior work. [15] The X-ray intensity distribution in the focal plane was finally summed on a uniform grid, and the results were obtained by tracing 10^9 photons using a Monte Carlo method. The bandwidth of the energy of the photons used was 0–330 keV.

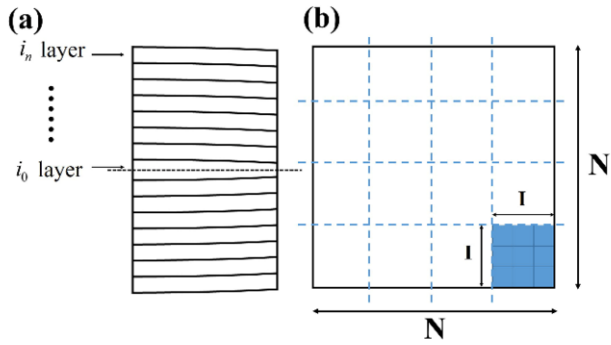

Figure 1. (a) Schematic structure of a polycapillary X-ray lens with square channels in the longitudinal direction; (b) Sectioned cross-section of the optic, $N=\{1,2,3...,n\}$ is the number of sections with spatially variant PSFs and $I=\{1,2,3...,i\}$ is the number of channels in one individual section.

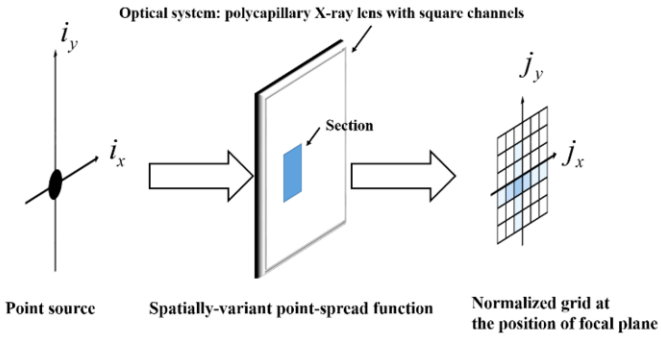

Figure 2. Calculation model of the spatially variant PSFs.

2.2. Simulation of the imaging experiment

The test object is shown in Fig. 3(a); it contains three letters, “BNU”, which is the abbreviation of Beijing Normal University. The whole object was set as an extended source of intensity of only the energy of interest. The contrast of the test object was calculated using the Michelson formula [16] $\frac{I_{\max}-I_{\min}}{I_{\max}+I_{\min}}$. It represents the count rates of the primary X-rays emitted from different parts of the object. For example, the ratio of the feature “BNU” to the background was set to 0.55:0.45, and the contrast value was 0.1. In terms of the geometric model of the optic, random channel tilts with a root mean square (RMS) value of 0.1 mrad and surface roughness with an RMS of 2 nm were considered. The manufacturing material was borosilicate glass. Further parameters of the simulation model are listed in Table 1. Our primary tool of investigation is based on the

Monte-Carlo ray-tracing method. The code has performed successfully in the numerical calculation of polycapillary X-ray lenses, as the results agreed well with experiments. [15],[17] Based on the code, a simulation of an imaging experiment was conducted. A schematic diagram of the simulation is shown in Fig. 3(b). The centers of the object, the lens and the confocal plane are coaxial. In the longitudinal direction, the object was positioned sufficiently far from the entrance of the lens. Therefore, the incident rays can be viewed as quasi-parallel in the case of paraxial approximation. The distance between the lens exits and the focal plane was determined using the optical properties of the lens. Table 2 shows the parameters of the simulation of the imaging experiment. In the simulation process, primary X-rays were emitted from random positions with a sampling frequency corresponding to the intensity of the object associated with the contrast value. Then, the rays struck the optic with random angles, and the final results were collected with a uniform grid in the focal plane after all the rays traced through the optic and exited.

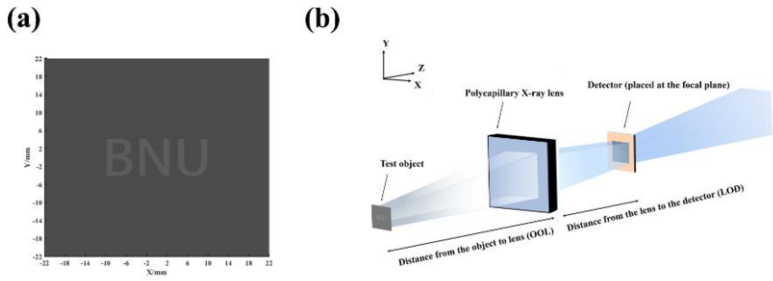

Figure 3. (a) Test object: the ratio of the feature BNU to the background was set to 0.55:0.45, and the contrast value was 0.1; (b) Schematic diagram of the simulation of the imaging experiment.

Table 1. Lens information

Type of glass	Borosilicate
Composition[wt%]	SiO_2-70, B_2O_3-25, Na_2O-2, Al_2O_3-2, K_2O-1
Density[g/cm^3]	2.28
Side length of the entrance[mm]	44
Side length of the exit[mm]	42
Thickness of the lens[mm]	10
Number of micro square channels	2200×2200
Channel diameter[μm]	20
Fractional open area	0.8

Table 2. Simulation of imaging experiment

Parameter	Value
OOL[mm]	10000
LOD[mm]	740
Ratio of feature to background (Contrast)	0.75:0.25 (0.5), 0.6:0.4 (0.2), 0.55:0.45(0.1), 0.505:0.495(0.01)
Number of rays	107, 108, 109, 1010
X-ray Energy	0–30 keV

2.3. Restoration method

As mentioned above, the sectioned method was selected in this work. The raw image viewed through the polycapillary X-ray lens with square channels was divided into tiles

of size $N\times N$ corresponding to the calculation of the spatially variant PSFs. Then, the restoration was performed for each tile individually. For a test object that emitted incoherent X-rays, the data collected in the detector plane satisfy a Poisson distribution. Taking no account of stochastic processes, the Poisson distributed signals can be expressed by:

$$Y(\mathbf{j})=\sum_{\mathbf{I}}H(\mathbf{j}\,|\,\mathbf{i})X(\mathbf{i}) \tag{1}$$

where $\mathbf{j}=\{j_1,j_2\}$ is the index of the pixels in the detector, $\mathbf{J}=\{\mathbf{j}_1,\mathbf{j}_2,\ldots,\mathbf{j}_n\}$ is the number of pixels in the detector and $\mathrm{Y}(\mathbf{j})$ represents the data acquired by the $\mathbf{j}th$ pixel of the detector. The term $\mathbf{i}=\{i_1,i_2\}$ is the index of the pixels in the plane of the test object, $\mathbf{I}=\{\mathbf{i}_1,\mathbf{i}_2,\ldots,\mathbf{i}_n\}$ is the number of pixels in the plane of the test object and $\mathrm{X}(\mathbf{i})$ is the object's true intensity. $\mathrm{H}(\mathbf{j}\,|\,\mathbf{i})$ is the PSF of the optical system. The mean of $\mathrm{Y}(\mathbf{j})$ is:

$$\mu(\mathbf{j})=\varepsilon(\mathbf{j})\sum_{\mathbf{J}}H(\mathbf{j}\,|\,\mathbf{i})X(\mathbf{i}) \tag{2}$$

where $\varepsilon(\mathbf{j})$ is defined as the transmission efficiency of each section of the lens.

Then, based on the prior information offered by $\mathrm{Y}(\mathbf{j})$, we employed a Lucy-Richardson overlap-save method using total variation (LROS-TV) to conduct the process of restoration. The basis of the LROS-TV method is the Lucy-Richardson deconvolution algorithm. In this work, the estimation of $\mathrm{X}(\mathbf{i})$ can be obtained by iteration using the LR algorithm:

$$\hat{X}^{p+1}(\mathbf{i})=\hat{X}^{p}(\mathbf{i})\frac{1}{\sum_{\mathbf{J}}\varepsilon(\mathbf{j})H(\mathbf{j}\,|\,\mathbf{i})}\sum_{\mathbf{J}}\frac{H(\mathbf{j}\,|\,\mathbf{i})}{\sum_{\mathbf{I}}H(\mathbf{j}\,|\,\mathbf{i})\hat{X}^{p}(\mathbf{i})}Y(\mathbf{j}) \tag{3}$$

where p is the iteration number. In the regulation step of the Lucy-Richardson algorithm, total variation (TV) helps to preserve the borders and suppresses the noise. This results in dividing the image $\hat{X}^{p}(\mathbf{i})$ in Eq. (3) by a factor and Eq. (3) becomes:

$$\hat{X}^{p+1}(\mathbf{i})=\frac{\hat{X}^{p}(\mathbf{i})}{1\text{-}\lambda\mathrm{div}\left(\dfrac{\nabla\hat{X}^{p}(\mathbf{i})}{\left|\nabla\hat{X}^{p}(\mathbf{i})\right|}\right)}\frac{1}{\sum_{\mathbf{J}}\varepsilon(\mathbf{j})H(\mathbf{j}\,|\,\mathbf{i})}\sum_{\mathbf{J}}\frac{H(\mathbf{j}\,|\,\mathbf{i})}{\sum_{\mathbf{I}}H(\mathbf{j}\,|\,\mathbf{i})\hat{X}^{p}(\mathbf{i})}Y(\mathbf{j}) \tag{4}$$

After termination of the iteration, the estimation of the original intensity in each tile is stitched together using the overlap-save method.

3. Experimental measurement

A photograph of the experimental setup is shown in Fig. 4(a). The experimental setup was arranged as shown in Fig. 4(b). An X-ray tube with a Cu target [MCBM 50-0.6B, RTW] was controlled using a five-dimensional alignment stage, and the focal spot size of the X-ray was 50 μm . The polycapillary X-ray lens with square channels used in this experiment had 900×900 square channels, and the ratio of open area was 0.65. The side length of the entrance plane of the lens was 26 mm. To estimate the spatially variant PSFs of the lens, a 10 μm pinhole was attached in front of the X-ray tube as a point object. The distance between the lens entrance and the Be window of the X-ray tube was set to 1000 mm. Then, the lens was sectioned to $N \times N = 9 \times 9$ with $I \times I = 100 \times 100$ channels in each section. The X-ray tube with the attached pinhole was moved at each step to ensure that the point object and the center of each section were coaxial. The images were recorded by an X-ray camera [C11440-42U30, HAMAMATSU]. The PSFs were obtained through deconvolution of these images and normalized to an energy of one. The test object of the simulation was replaced with an X-ray resolution chart [JIMA] in this experiment. A part of the chart was used, and the test object contained three 40 μm width and three 30 μm width stripes. The side length of the test object was 810 μm . The distance between the X-ray tube and the chart was 50 mm. The lens was placed 950 mm away from the chart, and the camera was placed in the focal plane at a distance of 200 mm away from the lens exit. The voltage of the tube was set to 30 kV, and the current was set to 300 μA , 400 μA , 500 μA and 600 μA . The exposure time was set to 180 s for all of these cases.

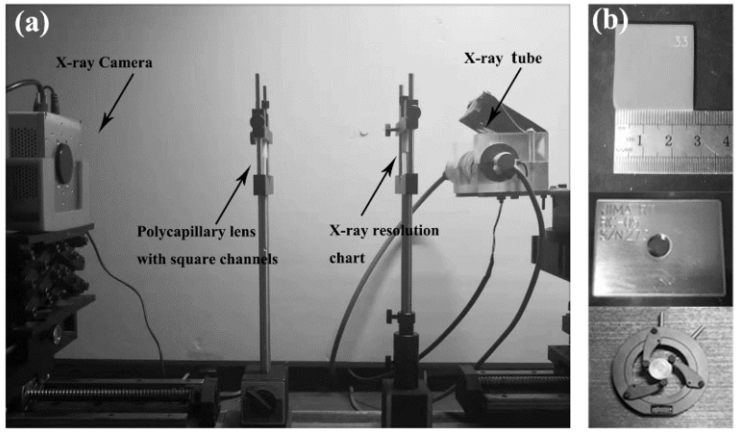

Figure 4. (a) Experimental setup; (b) From top to bottom: polycapillary X-ray lens with square channels, X-ray resolution chart and pinhole.

To test the feasibility of the LROS-TV method, a simple imaging experiment was conducted. Fig. 5(a) shows the estimated spatially variant PSFs. Fig. 5(b) shows the features of the resolution chart. Due to manufacturing errors such as dislocation and tilt of the channels, the PSFs cannot provide complete prior information for the process of restoration. In Fig. 6, (a)-(d) are the images of the resolution chart photographed directly by the camera, (e)-(h) are the raw images viewed through the lens and (i)-(l) are the deconvolved images using the LROS-TV method with 1000 iterations. With increased

current values, the contrast of the test object improved. The features of images projected back to the object plane can be better resolved. The PSNRs of Fig. 6(i)-(l) were 22.8382, 21.4842, 20.4325 and 19.8256, respectively. The X-ray source spot size increases with increasing current.

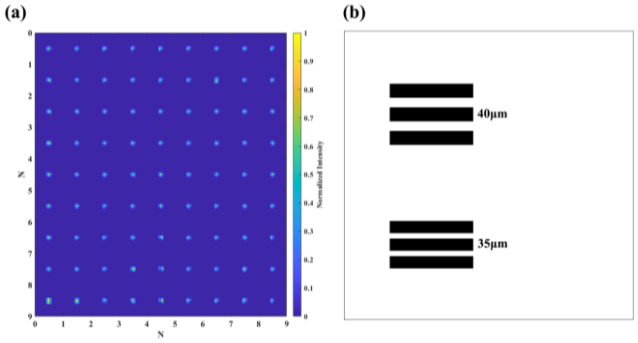

Figure 5. (a) Experimental spatially variant PSFs; (b) Pattern of the X-ray resolution chart JIMA.

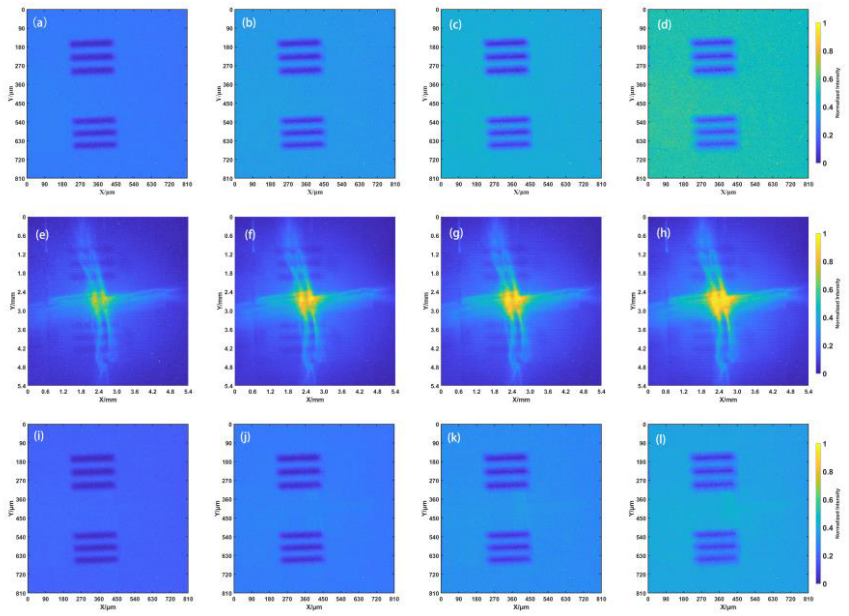

Figure 6. (a)-(d) Images of the resolution chart photographed directly by the camera; (e)-(h) Raw images viewed by the polycapillary X-ray lens with square channels recorded by the X-ray camera in the case of same voltage and different currents, from left to right the value is : 30kV 300 μA , 30kV 400 μA , 30kV 500 μA , 30kV 600 μA ; (i)-(l) Corresponding deconvolved images at the object plane.

4. Conclusion

In summary, we presented an idea to recover real images of an object from the raw data viewed through a polycapillary X-ray lens with square channels using the LROS-TV method. Because the curvature of each channel has tiny differences, the concept of a spatially variant point spread function was used in this work, and the whole lens was sectioned for simplified calculation. Using the prior information provided by the PSFs, imaging restoration was investigated by changing the numbers of photons that strike the lens and the contrast value of the test object. A feature can be clearly distinguished from the background when projected back to the object plane at the 109-photon level.

In addition, a simple coaxial imaging experiment was implemented to test the feasibility of the LROS-TV method. The results validated the method used in imaging restoration. The errors caused by lens manufacturing errors and the limited numbers of sections for simplified calculations make the next goal of our work clear. Methods to eliminate artifacts should also be investigated for better restoration quality. On the one hand, the manufacturing technique should be improved for a more satisfactory geometric structure. On the other hand, a more precise model for PSF estimation should be established, and parallel computing programs should be used. Furthermore, this work indicates that a polycapillary X-ray lens with square channels can be used as a lens for X-ray imaging transmission.

References

[1] Kumakhov MA. Radiat EffDefect S. 1991. p. 329-363.
[2] Schields PJ, Gibson DM and Gibson WM. Powder Diffr. 2002. p. 70-80.
[3] Yonehara T, Yamaguchi M and Tsuji K. Spectrochim Acta B. 2010. p. 441-444.
[4] Sun TX, Zhang ML and Liu ZG. J Synchrotron Radiat. 2009. p. 116-118.
[5] Dabrowski KM, Dul DT and Wrobel A. Appl Phys Lett. 2013. p. 102.
[6] Dabrowski KM, Dul DT and Korecki P. Opt Express. 2013. p. 2920-2927.
[7] Qin M, Yi LT and Pan K. Opt Commun. 2018. p. 205-210.
[8] Yi LT, Liu ZG. and Li ZB. Opt Commun. 2019. p. 139-142.
[9] Peele AG. Nucl Instrum Meth A. 2001. p. 354-341.
[10] Trussell HJ, Hunt BR. Ieee T Acoust Speech. 1978. p. 608-609.
[11] Trussell HJ, Hunt BR. Ieee T Acoust Speech. 1978. p. 157-164.
[12] Cobb ML, Hertz PL and Whaley RO. Digital Image Recovery and Synthesis II. 1993. p. 202-208.
[13] Ozkan MK, Tekalp AM and Sezan MI. Ieee T Image Process. 1994. p. 450-454.
[14] Marrugo AG, Millan MS and Sorel M. J Biomed Opt. 2014.
[15] Peng SQ, Liu ZG and Sun TX. Chinese Phys B. 2016.
[16] Pelli DG, Bex P. Vision Res. 2013. p. 10-14.
[17] Peng SQ, Liu ZG and Sun TX. Nucl Instrum Meth A. 2015. p. 186-191.